Double Diffusive Mixed Convection with Thermodiffusion Effect in a Driven Cavity by Lattice Boltzmann Method

Soufiene Bettaibi[(✉)] and Omar Jellouli

Laboratoire des Energies Renouvelable et Matériaux Avancés (LERMA),
Université Internationale de Rabat (UIR), Rocade Rabat-Salé,
11100 Rabat-Sala El Jadida, Morocco
bettaibisoufiene@gmail.com, jellouliomar@gmail.com

Abstract. We perform a numerical study of thermal diffusion effects on double-diffusive mixed convection in a lid-driven square cavity, differentially heated and salted. The fluid flow is solved by a multiple relaxation time (MRT) lattice Boltzmann method (LBM), whereas the temperature and concentration fields are computed by finite difference method (FDM). To assess numerical accuracy, the model (MRT-LBM coupled with FDM) are verified and validated using data from the literature. Besides reasonable agreement, satisfactory computational efficiency is also found. Thereafter, the model is applied for the thermal diffusion effect on a double-diffusive mixed convection in a cavity with moving lid. Results are obtained depending on various dimensionless parameters. It is found that upon increasing the Soret number, heat transfer is slightly enhanced whereas the thickness of the concentration boundary layer increases, thereby decreasing the mass transfer rate.

Keywords: Lattice Boltzmann method (LBM) · Finite difference method (FDM) · Thermodiffusion effect · Double diffusive mixed convection

1 Introduction

In the last few years an alternative numerical method has attracted much attention as a technique in fluid engineering. This method called Lattice Boltzmann Method (LBM) is a mesoscopic method. The fundamental idea behind LBM is to establish a simplified kinetic model to obey the corresponding macroscopic, i.e. Navier Stokes, equations. It has proved its capability to simulate a large variety of fluid flows [1–4]. The LBM has become a very successful alternative numerical method for computational fluid dynamics. Moreover, it is well suited for high-performance implementations on massively parallel processors, including graphics processing units [5]. The lattice Boltzmann method comes with two main collision models. One of the simplest and most widely used proposed by

Bhatnagar, Gross and Krook [6] called BGK model, is based on a single relaxation time (SRT) and proves very simple and efficient for simulating fluid flows. Up to now, the lattice Boltzmann equation with the BGK collision operator is still the most popular lattice Boltzmann method. Despite many advantages, the BGK model reveals some deficiencies due to numerical instabilities [7] and consequent difficulties to reach high Reynolds number flows. The second model called MRT operator [8] where each relaxation rate can be tuned independently, presents some advantages compared to the BGK model in terms of numerical stability. Because of this, the MRT-LBM has become increasingly popular in the recent years.

For solving thermal LBM model, several approaches have been proposed, which can be grouped into four categories: passive-scalar approach, multispeed-approach, double-population approach and hybrid approach. The multispeed approach consists in using only one distribution function for treating all thermo-hydrodynamic equations [9–11]. The passive scalar approach consists of treating temperature as the current along an extra-spatial dimension [12]. It is efficient, but being related to the four-dimensional lattices used in the earliest days of LBM research, it has somehow lost popularity The multi-speed model is most natural, but requires additional discrete speeds and is prone to numerical instabilities. The double population approach [13,14] makes use two independent functions for thermo-hydrodynamic equations. This model assumes that, the viscous dissipation and compression work can be neglected for incompressible fluids and the evolution of the temperature is given by the advection-diffusion Eq. [15,16]. This approach shows significant improvements in numerical stability, but to the cost of introducing an additional distribution function to simulate a passive scalar. The hybrid approach [16] used in this article, consists of leaving LBM only for the flow solution, while the energy equation is solved by a different numerical method, typically finite-differences or finite-volumes.

For this reason, in our work the LBM-MRT model is used for velocity field, on the one hand, and finite differences for temperature and concentration fields, on the other hand.

Thermosolutal buoyancy-driven flow in confined cavities represents a fundamental problem, with many engineering applications, such as pollutant transport, nuclear reactor cooling, cooling of electronic systems, to name but a few. Double-diffusive heat and mass transfer problems can be classified as problems involving natural convection, forced convection and combination of both, often referred to as mixed convection [17–22].

Diffusion of heat due to a mass concentration gradients (Dufour effect) and diffusion of matter induced by temperature gradients (Soret effect) are the subject of intensive research, due to the broad range of application in technology and engineering. These include mixture between gases, oil-reservoirs, isotope separation and many others [23–29].

For all the above cited works, the authors have used several configurations to study both the double-diffusive natural and mixed convection problems. Moreover, they applied different numerical methods to solve the basic thermo-fluid

equations. Comparatively less attention has been given to the problem of a double-diffusive mixed convection with Soret effect in a driven cavity. From this point of view and to the best of the authors knowledge, no attention has been paid to explore the thermal diffusion effect (Soret effect) on a double-diffusive mixed convection in a cavity with moving lid, using the lattice Boltzmann method (LBM).

In this paper we present a numerical model for double-diffusive mixed convection with Soret effect in a lid-driven cavity. This model uses the Lattice Boltzmann method with multiple relaxation time for collision operator to simulate mass and momentum conservation and finite differences to compute the temperature and concentration fields. We also attempt to provide benchmark quality results on CPU time which can be compared with the existing data.

2   Mathematical Model

2.1   Definition of the Problem

The physical model under consideration is presented in Fig. (1). The two-dimensional lid-driven cavity has height H and width L (Aspect ratio $Ar = \frac{H}{L}$), the vertical side walls are thermally insulated and the top wall moves at a constant velocity $U_0 = 0.1$. The bottom and top walls are maintained at two different but uniform temperatures and concentrations such that the top wall has the temperature T_c and concentration C_c, while the bottom wall has the temperature T_h and concentration C_h, respectively, where $T_h > T_c$ and $C_h > C_c$.
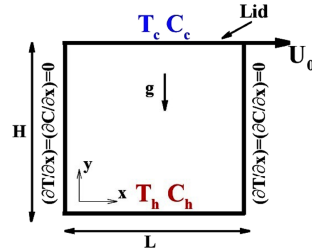

Fig. 1. Geometry of the enclosure and coordinate system.

The thermophysical properties of the fluid are assumed to be constant except for the density variation in the buoyancy term according to the Boussinesq approximation:

$$\rho = \rho_0 \left(1 - \beta_T \left(T - T_m\right) - \beta_S \left(C - C_m\right)\right)$$

where ρ_0 is the fluid density at the reference temperature $T_m = \left(\frac{T_h + T_c}{2}\right)$ and concentration $C_m = \left(\frac{C_h + C_c}{2}\right)$, β_T and β_S are the thermal and mass expansion coefficients, respectively.

To solve the problem of double-diffusive mixed convection with Soret effect in a lid-driven cavity we assume: a Newtonian incompressible fluid, the Boussinesq approximation for buoyancy, viscous heating and compression work are neglected and no source term inside the cavity.

Based on these assumptions, the dimensional governing equations of mass and momentum are solved by the MRT lattice Boltzmann Method (MRT-LBM) while energy and species equations are solved by Finite Difference Method (FDM).

The non dimensional terms used in this work like thermal Grashof number, the solutal Grashof number, the buoyancy ratio, the Richardson number, the Reynolds number, the Prandtl number, the Schmidt number and the Soret number are defined, respectively, by:

$$G_{RT} = g\beta_T \left(\frac{(T_h - T_c) H^3}{\nu^2} \right); \ G_{RS} = g\beta_S \left(\frac{(C_h - C_c) H^3}{\nu^2} \right)$$

$$N = \frac{\beta_S (C_h - C_c)}{\beta_T (T_h - T_c)} = \frac{G_{RS}}{G_{RT}}$$

$$Ri = \frac{G_{RT}}{Re^2}; \qquad Re = \frac{U_0.H}{\nu}; \qquad Pr = \frac{\nu}{\alpha}; \qquad Sc = \frac{\nu}{D}$$

$$Sr = \frac{D.K_T (T_h - T_c)}{T_m \nu (C_h - C_c)}$$

The average Nusselt and Sherwood numbers, defined by temperature and concentration gradients at walls, are calculated via:

$$Nu_{av} = -\frac{1}{T_h - T_c} \int_0^H \left(\frac{\partial T}{\partial y} \right)_{wall} dx$$

$$Sh_{av} = -\frac{1}{C_h - C_c} \int_0^H \left(\frac{\partial C}{\partial y} \right)_{wall} dx$$

The dimensionless variables governing this problem are U the x-component velocity and V the y-component velocity.

The following dimensionless quantities are given by:

$$U^* = \frac{U}{U_0} \qquad V^* = \frac{V}{U_0} \qquad \theta = \frac{T - T_c}{T_h - T_c} \qquad t^* = \frac{tU_0}{H} \qquad \Theta = \frac{C - C_c}{C_h - C_c}$$

2.2   MRT-LBM Hybrid Model for Fluid Flow

Within this approach, fluid is described by a particle distribution function which evolves in discrete space and time (a $D_d Q_q$ lattice; d dimensions and q velocities) following two steps: propagation and collision. Hence, the lattice Boltzmann equation is expressed as:

$$f_i \left(\overrightarrow{x} + \overrightarrow{e_i}, t + 1 \right) - f_i \left(\overrightarrow{x}, t \right) = \Omega_i \qquad (1)$$

where f_i is the probability of finding a particle at lattice node $\overrightarrow{x}$, at the time t, moving with velocity $\overrightarrow{e_i}$ ($i = 0, ...q - 1$) and Ω_i is the collision operator. Note that the time step is made unit by convention.

The Lattice Boltzmann equation with multiple relaxation time (MRT) can be expressed as:

$$f_i \left(\overrightarrow{x} + \overrightarrow{e_i} \Delta t, t + \Delta t \right) = f_i \left(\overrightarrow{x}, t \right) - M^{-1} S_{ij} \left[m_j - m_{ij}^{eq} \left(\overrightarrow{x}, t \right) \right] \qquad (2)$$

M is a transform matrix projecting the discrete distribution function f into moment space $|m\rangle = M.|f\rangle$, m_j^{eq} is the equilibrium moment.

The physical meaning of the moments is as follows:

$$|m\rangle = \left(\rho \; e \; j_x \; j_y \; \epsilon \; q_x \; q_y \; p_{xx} \; p_{xy} \right)^{\top} \tag{3}$$

where ρ is the density, e is the energy, j_x and j_y the x and y components of momentum (mass flux) and ϵ is defined as the kinetic energy, q_x and q_y are the x and y components of the energy flux. In addition, p_{xx} and p_{xy} correspond to the diagonal and off-diagonal components of the viscous stress tensor, and $\top$ denotes the transpose operator.

The macroscopic fluid variables, density ρ and velocity $\overrightarrow{u}$ are obtained from the moments of the distribution functions as follows:

$$\rho = \sum_{i=0}^{q-1} f_i \qquad and \qquad \rho \overrightarrow{u} = \sum_{i=0}^{q-1} f_i \overrightarrow{e_i} \tag{4}$$

For the (D_2Q_9) lattices(Fig(2)), the nine discrete velocities $\overrightarrow{e_i}$ are defined as:

$$\begin{cases} \overrightarrow{e_i} = \overrightarrow{0} & i = 0 \\ \overrightarrow{e_i} = \left(\cos\left[(i-1)\frac{\pi}{2}\right], \sin\left[(i-1)\frac{\pi}{2}\right] \right) c & i = 1,2,3,4 \\ \overrightarrow{e_i} = \left(\cos\left[(2i-9)\frac{\pi}{4}\right], \sin\left[(2i-9)\frac{\pi}{4}\right] \right) c\sqrt{2} & i = 5,6,7,8 \end{cases} \tag{5}$$

Where ΔX and Δt are the lattice width and time step, respectively. It is chosen that $\Delta X = \Delta t$, thus $c = \frac{\Delta X}{\Delta t} = 1$ is the lattice speed.

With a (D_2Q_9) lattices, the transformation matrix M and the moment vector m are defined as:
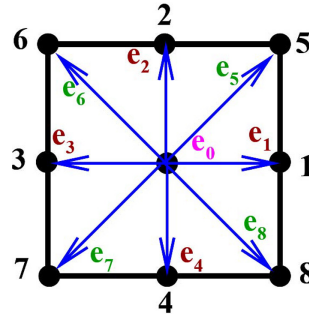

Fig. 2. Lattice structure for the D_2Q_9 model.

$$m = \begin{bmatrix} \rho \\ e \\ \epsilon \\ j_x \\ j_y \\ q_x \\ q_y \\ p_{xx} \\ p_{xy} \end{bmatrix} \begin{bmatrix} 1 & 1 & 1 & 1 & 1 & 1 & 1 & 1 & 1 \\ -4 & -1 & -1 & -1 & -1 & 2 & 2 & 2 & 2 \\ 4 & -2 & -2 & -2 & -2 & 1 & 1 & 1 & 1 \\ 0 & 1 & 0 & -1 & 0 & 1 & -1 & -1 & 1 \\ 0 & -2 & 0 & 2 & 0 & 1 & -1 & -1 & 1 \\ 0 & 0 & 1 & 0 & -1 & 1 & 1 & -1 & -1 \\ 0 & 0 & -2 & 0 & 2 & 1 & 1 & -1 & -1 \\ 0 & 1 & -1 & 1 & -1 & 0 & 0 & 0 & 0 \\ 0 & 0 & 0 & 0 & 0 & 1 & -1 & 1 & -1 \end{bmatrix} \begin{bmatrix} f_0 \\ f_1 \\ f_2 \\ f_3 \\ f_4 \\ f_5 \\ f_6 \\ f_7 \\ f_8 \end{bmatrix} = M.f \tag{6}$$

Where the equilibrium value of moments can be defined from the following equations:

$$\begin{cases} \rho^{eq} = \rho \\ e^{eq} = -2\rho + 3\left(u^2 + v^2\right) \\ \epsilon^{eq} = \rho - 3\left(u^2 + v^2\right) \\ j_x^{eq} = \rho u \\ j_y^{eq} = \rho v \end{cases} \quad and \quad \begin{cases} q_x^{eq} = -u \\ q_y^{eq} = -v \\ p_{xx}^{eq} = u^2 - v^2 \\ p_{xy}^{eq} = uv \end{cases} \tag{7}$$

The equilibrium density distribution function, which depends on the local fluid velocity and density is given by:

$$f_i^{eq} = w_i \rho \left[1 + \frac{3\overrightarrow{e_i}.\overrightarrow{u}}{c^2} + \frac{9\left(\overrightarrow{e_i}.\overrightarrow{u}\right)^2}{2c^4} - \frac{3\overrightarrow{u}.\overrightarrow{u}}{2c^2}\right] \qquad i = 0 \rightarrow 8 \tag{8}$$

Where w_i is the weighting factor defined as:

$$\begin{cases} w_i = \frac{4}{9} & i = 0 \\ w_i = \frac{1}{9} & i = 1, 2, 3, 4 \\ w_i = \frac{1}{36} & i = 5, 6, 7, 8 \end{cases} \tag{9}$$

The diagonal relaxation matrix can be written as:

$$S = diag\left[S_0, S_1, S_2, S_3, S_4, S_5, S_6, S_7, S_8\right] \tag{10}$$

In the present work, we assume $S_0 = S_3 = S_5 = 0$ for both the mass and momentum conservation before and after collision. We also consider $S_7 = S_8 = \frac{1}{\tau}$ due to fact that the viscosity formulation is the same as SRT model. In the present simulation $S_1 = 1.64$, $S_2 = 1.2$ and $S_4 = S_6 = 8 \times \frac{(2-S_7)}{(8-S_7)}$.

It should be noted that in the LBM the kinematic viscosity ν is related to the relaxation time by the following relation:

$$\nu = (\tau - 0.5)\,c_s^2 \Delta t \tag{11}$$

Where $c_s = \frac{c}{\sqrt{3}}$ is the speed of sound. For the (D_2Q_9) lattices the viscosity is positive which requires the choice of $\tau > 0.5$.

2.3   Finite Difference Method (FDM) for Temperature and Concentration Fields

Equation (4) is discretized by the Finite Difference Method (FDM) using the Taylor series expansion of the second order. To improve the stability of the hybrid model used in this article, Lallemand and Luo [16] suggest using a discretization in accordance with discretization speeds. They proposed the following discretization for the derivatives with $(\Delta x = \Delta t = 1)$:

For more clarity, in the following the variable (Φ) designates the temperature (T) or the concentration (C). Therefore, the equations for both scalars $(T$ and $C)$ can be written as:

$$\frac{\partial \Phi}{\partial x} = \left(\Phi_{i+1,j} - \Phi_{i-1,j} - \frac{1}{4}\left[\Phi_{i+1,j+1} - \Phi_{i-1,j+1} + \Phi_{i+1,j-1} - \Phi_{i-1,j-1}\right]\right) \tag{12}$$

$$\frac{\partial \Phi}{\partial y} = \left(\Phi_{i,j+1} - \Phi_{i,j-1} - \frac{1}{4} \left[\Phi_{i+1,j+1} - \Phi_{i-1,j+1} + \Phi_{i+1,j-1} - \Phi_{i-1,j-1} \right] \right) \quad (13)$$

And for Laplacian:

$$\nabla^2 \Phi = \left(\left[\Phi_{i+1,j} + \Phi_{i,j+1} + \Phi_{i-1,j} \right] \right.$$
$$\left. - \frac{1}{2} \left[\Phi_{i+1,j+1} + \Phi_{i-1,j+1} + \Phi_{i-1,j-1} + \Phi_{i+1,j-1} \right] - 6\Phi_{i,j} \right) \quad (14)$$

For the time derivative, we use an explicit difference scheme. Then for the solution is conditionally stable:

$$\frac{\partial \Phi}{\partial t} = \left(\Phi_{i,j}^{n+1} - \Phi_{i,j}^{n} \right) \quad (15)$$

Substituting the Eqs. (12–15) to Eq. (4) or (5):

$$\begin{aligned}
\Phi_{i,j}^{n+1} = {}& \Phi_{i,j}^{n} \left(1 - 6\alpha \right) + \Phi_{i+1,j}^{n} \left(-u + 2\alpha \right) + \Phi_{i-1,j}^{n} \left(u + 2\alpha \right) \\
& + \Phi_{i,j+1}^{n} \left(-v + 2\alpha \right) + \Phi_{i,j-1}^{n} \left(v + 2\alpha \right) \\
& + \Phi_{i+1,j+1}^{n} \left(\tfrac{1}{4}u + \tfrac{1}{4}v - \tfrac{1}{2}\alpha \right) \\
& + \Phi_{i-1,j+1}^{n} \left(-\tfrac{1}{4}u + \tfrac{1}{4}v - \tfrac{1}{2}\alpha \right) \\
& + \Phi_{i+1,j-1}^{n} \left(\tfrac{1}{4}u - \tfrac{1}{4}v - \tfrac{1}{2}\alpha \right) \\
& + \Phi_{i-1,j-1}^{n} \left(-\tfrac{1}{4}u - \tfrac{1}{4}v - \tfrac{1}{2}\alpha \right)
\end{aligned} \quad (16)$$

The coefficient that accompanies $(\Phi_{i,j})$ in the above equation plays an important role for explicit schemes. These schemes are conditionally stable and then lead to constraints on the time step and space step choices. One of the required stability conditions for the current scheme is taken when the thermal diffusivity and viscosity are related to Prandtl number and limited by:

$$(1 - 6\alpha) \geq 0 \Rightarrow \alpha = \frac{\nu}{Pr} \leq \frac{1}{6}$$

On the other hand, the stability conditions of the scheme relative to the mass diffusivity and viscosity are related to Lewis number and limited by:

$$(1 - 6D) \geq 0 \Rightarrow D = \frac{\nu}{Le} \leq \frac{1}{6}$$

2.4   Boundary Conditions

In the present work, we consider two types of boundary conditions. We apply the Dirichlet boundary conditions (fixed temperature and concentration) at horizontal walls while the vertical walls are adiabatic, defined by:

$$\begin{aligned}
U = V = 0, \quad & \theta = \Theta = 1 \quad \text{at} \quad Y = 0, \quad 0 \leq X \leq 1 \\
U = 0.1, \quad V = 0, \quad & \theta = \Theta = 0 \quad \text{at} \quad Y = 1, \quad 0 \leq X \leq 1 \\
U = V = 0, \quad & \frac{\partial \theta}{\partial X} = \frac{\partial \Theta}{\partial X} = 0 \quad \text{at} \quad X = 0, \quad 0 \leq Y \leq 1 \\
U = V = 0, \quad & \frac{\partial \theta}{\partial X} = \frac{\partial \Theta}{\partial X} = 0 \quad \text{at} \quad X = 1, \quad 0 \leq Y \leq 1
\end{aligned}$$

The no slip boundary condition is imposed at all walls. This type of boundary condition in the LBM is achieved half-way between the boundary nodes [17]. As a result, an extrapolation is needed on boundary nodes to enforce the correct thermal boundary conditions.

The following expressions were used to impose the temperature (the same procedure for the concentration):

$$T_{i,0} = \frac{8}{3}T_{wall} - 2T_{i,1} + \frac{1}{3}T_{i,2} \tag{17}$$

For adiabatic boundary conditions at the walls:

$$T_{0,j} = \frac{21}{23}T_{1,j} + \frac{3}{23}T_{2,j} + \frac{1}{23}T_{3,j} \tag{18}$$

3   Model Validation

In order to check the validity of the proposed model, Table 1, reports a comparison of our numerical results with those of Ben Cheikh et al. [30] in terms of CPU time and number of steps for different grid sizes and for Rayleigh number $Ra = 10^5$. These authors used a finite volume multigrid method and compared two different schemes namely, the accelerated finite volume full multigrid method (AFMG) and the red and black successive overrelaxation scheme (RBSOR) inorder to study convective flow in a square differentially heated cavity, the top and bottom walls are thermally insulated whereas the west and east walls are maintained isothermally at constant and temperatures T_h (hot) and T_c (cold), respectively. It is to be noted that the CPU time performances obtained on a dual-1.73 GHz processor. From this table it is seen that the present model is more efficient in CPU than the two schemes used for comparison and shows also an interesting gain concerning in time step-size. Of course these data should be taken as a semi-quantitative indication, a more detailed comparison requiring the consideration of many parameters, including code optimization and related issues which are beyond the scope of this paper.

Concerning the double-diffusive mixed convection without Soret effect, a grid-dependence study was carried out by setting $Pr = 1$, $Le = 2$, $Re = 500$ and $G_{RT} = G_{RS} = 100$ ($N = 1$). Five uniform node resolutions, 31^2, 51^2, 61^2, 71^2 and 81^2 were examined.

In Fig. (3a–3b) we compare our results for the steady state velocity and temperature profiles along the mid-section of the cavity in the Y-direction, with the results of Al-Amiri et al. [21] obtained using stream function vorticity formulation. As shown from these figures, reasonable results are obtained using node a 81^2 grid resolution.

Thus, the present model is verified and validated with different numerical methods in the literature. The different comparisons indicate the effectiveness and accuracy of the proposed model. Next, the model is applied to the

Table 1. Comparison of CPU times and number of steps with Ref. [30] for different grid sizes, for $Ra = 10^5$.

Grid size	Method	Steps	CPU[s]	CPU[s]/Steps
	Present	67500	19	0.00028
$32 * 32$	AFMG [30]	5000	26	0.0052
	RBSOR [30]		33	0.0066
	Present	113800	139	0.00122
$64 * 64$	AFMG [30]	10000	209	0.021
	RBSOR [30]		450	0.045
	Present	128400	640	0.00498
$128 * 128$	AFMG [30]	20000	2300	0.115
	RBSOR [30]		18057	0.903
	Present	460400	09455	0.02053
$256 * 256$	AFMG [30]	40000	15595	0.390
	RBSOR [30]		632000	15.80

thermosolutal mixed convection with Soret effect in a cavity with moving top wall. We also endeavour to provide benchmark results to be compared with the existing data.
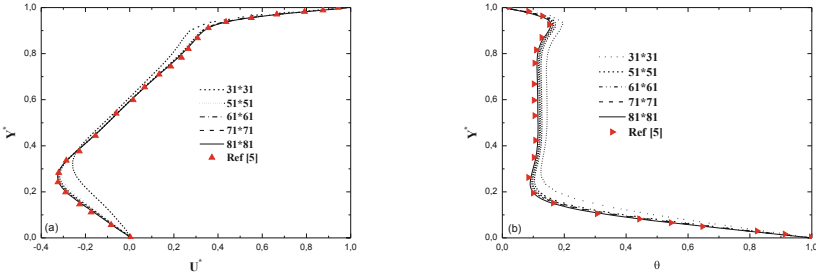
Fig. 3. Grid independence test for $G_{RS} = G_{RT} = 10^2$ ($N = 1$), $Le = 2$ and $Re = 500$, (a) U-Velocity and (b) Temperature.

4   Results of Thermosolutal Mixed Convection with Soret Effect

In this section we study the numerical procedure of MRT-LBM coupled with FDM for thermosolutal mixed convection with Soret effect in a lid-driven square

cavity. The fluid velocity is determined by D_2Q_9 MRT-LBM model while the temperature and concentration fields are computed by FDM. The effects of various parameters such as the Soret number Sr, the buoyancy number N on the flow structure and the heat and mass transfer as well as the average Nusselt and Sherwood numbers are calculated. The Schmidt number $Sc = 5$, the Prandtl number $Pr = 0.71$, the Reynolds number $Re = 316$ and the Richardson number is fixed at $Ri = 0.1$.
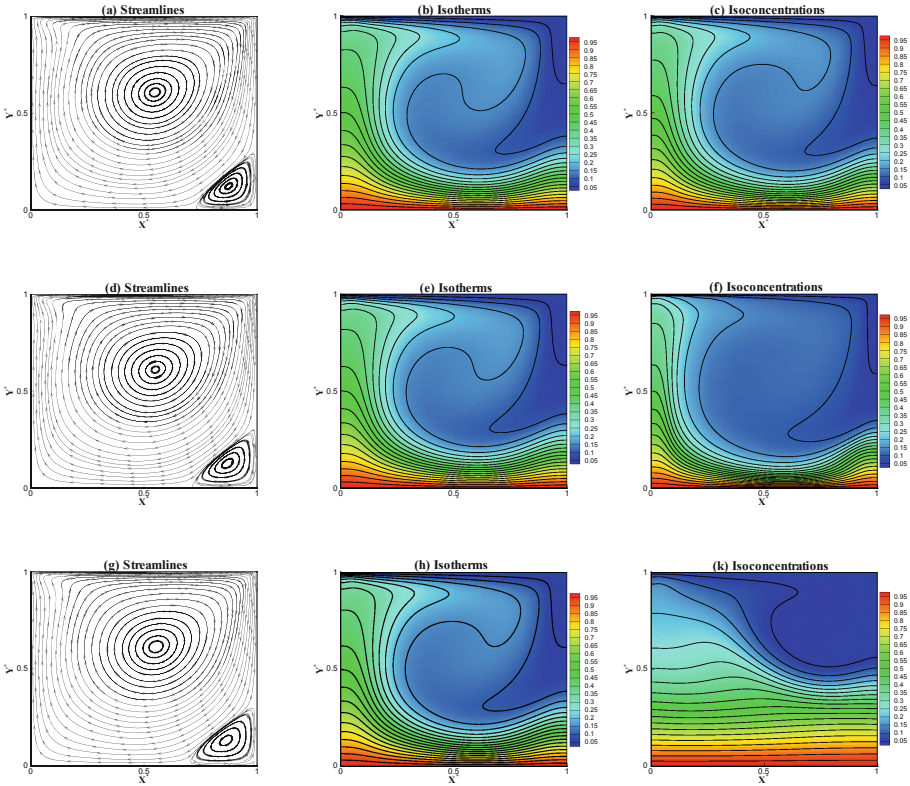

Fig. 4. Computed streamlines, isotherms and isoconcentrations: (a, d and c) for $Sr = 1$, (d, e and f) for $Sr = 0.5$, (g, h and k) for $Sr = 0$.

Effect of Soret Number Sr. In this subsection, numerical results are obtained for the thermal and solutal Grashof numbers fixed at $G_{RT} = G_{RS} = 10^5$ ($N = 1$), while the Soret number is changed in the range $Sr = 0, 0.5$ and 1. The results are reported in terms of streamlines, isotherms and isoconcentrations, respectively.

For $Sr = 0$, the problem reduces to a pure thermosolutal mixed convection. Fig(4a-4c) show the streamlines, isotherms and isoconcentrations predicted by the present hybrid lattice-Boltzmann finite difference simulation. As shown from

Fig. (4a), a primary circulation clockwise vortex occupies the whole volume of the cavity, with a secondary counterclockwise vortex that is formed near the bottom corners, due to the dominant effect of mechanically driven top lid to the entire cavity. The distribution of isotherms and isoconcentrations depicted in Fig. (4b–4c) show that there are steep temperature and concentration gradients in the vertical direction, near the bottom wall. By increasing the Soret number to $Sr = 0.5$ (Fig. (4d–4f)) and $Sr = 1$ (Fig. (4g–4k)), the flow patterns are characterized by a primary recirculating clockwise vortex, that occupies the bulk of the square cavity with a secondary counterclockwise vortex near the bottom corner, are the results of negative pressure gradient generated by the primary circulating fluid. In addition, steep temperature gradients are clustered in the vertical direction of the interior region and near the bottom wall. It is to be noted that, in this case, by increasing the Soret number, no significant effect is observed in terms of both streamlines and isotherms. Due to the significant dependence of the Sherwood number on the Soret number, we note a dramatic variation in the mass contours with thinner mass boundary layer forming along the wall (see Fig. (4f, 4k)). This is due to the increase in diffusivity upon increasing the values of the Soret number.

Table 2. Effect of Soret number Sr on the average Nusselt and Sherwood numbers for $G_{RT} = G_{RS} = 10^5$, $Re = 316$, $Sc = 5$ and $Ri = 0.1$.

Sr	Nu_{av}	Sh_{av}	CPU [s]	Steps
0	3.743	7.049	881.5	384500
0.5	3.809	5.773	815.4	353800
1	3.886	4.450	645	286200

This is also demonstrated from date in Table 2, in which we calculated the average Nusselt and Sherwood numbers for three values of the Soret number. One can note that, by increasing the Soret number from $Sr = 0$ to $Sr = 1$, the heat transfer represented by the Nusselt number is slightly increased. On the other hand, if the Soret parameter is increased, the thickness of the concentration boundary layer increases, thereby decreasing the mass transfer rate represented by the average Sherwood number.

Conclusion

In this paper we employ the lattice Boltzmann method with multiple relaxation time (MRT-LBM), coupled with the finite difference method (FDM) to simulate thermo-hydrodynamics. The fluid flow is computed by D_2Q_9 MRT model while the temperature and concentration fields are solved by FDM. The 2-D square differentially heated cavity and double-diffusive mixed convection without Soret effect was considered as validation test. Satisfactory agreement has

been obtained, compared with different numerical methods in the current literature. The results show that the present model can yield benchmark quality results. The employed model has then applied to a thermosolutal mixed convection with Soret effect in a cavity with moving top wall. Results show that the heat transfer represented by the average Nusselt number is slightly enhanced upon increasing the Soret number. Whereas, the mass transfer represented by the average Sherwood number is decreased by further augmenting the Soret number.

As a perspective of this work, this new model will be extended to three-dimensional problems. It could be also tested with a parallel implementation using graphics processing unit (GPU) and especially in the combined mode problems which are computationally very expensive. Work along this direction is underway.

References

1. Succi, S.: The Lattice Boltzmann - For Fluid Dynamics and Beyond, 288p. Oxford University Press, Oxford (2001)
2. Benzi, R., Succi, S., Vergassola, M.: The lattice Boltzmann equation: theory and applications. Phys. Rep. **22**, 145–197 (1992)
3. Wolf-Gladrow, D.A.: Lattice-Gas Cellular Automata and Lattice Boltzmann Models: An Introduction, p. 308p. Springer, Berlin (2000). https://doi.org/10.1007/b72010
4. Filippova, O., Hanel, D.: A novel BGK approach for low Mach number combustion. J. Comput. Phys. **158**, 139–160 (2000)
5. Kuznik, F., Obrecht, C., Rusaouen, G., Roux, J.J.: LBM based flow simulation using GPU computing processor. Comput. Math. Appl. **59**, 2380–2392 (2010)
6. Bhatnagar, P., Gross, E., Krook, M.: A model for collision processes in gases. I. Small amplitude processes in charged and neutral one-component systems. Phys. Rev. **94**, 511–525 (1954)
7. Lallemand, P., Luo, L.-S.: Theory of the lattice Boltzmann method: acoustic and thermal properties in two and three dimensions. Phys. Rev. E **68**(3 Pt 2), 036706 (2003). Epub 2003 Sep 23
8. d'Humières, D., Ginzburg, I., Krafczyk, M., Lallemand, P., Luo, L.: Multiple-relaxation-timel attice Boltzmann models in three dimensions. Philos. Trans. R. Soc. Math. Phys. Eng. Sci. 437–451 (2002)
9. Chen, Y., Ohashi, H., Akiyama, M.A.: Thermal lattice Bhatnagar-Gross-Krook model without nonlinear deviations in macrodynamic equations. Phys. Rev. E **50**, 2776–2783 (1994)
10. Pavlo, P., Vahala, G., Vahala, L., Soe, M.: Linear stability analysis of thermo-lattice Boltzmann models. J. Comput. Phys **139**, 79–91 (1998)
11. McNamara, G.R., Garca, A.L., Alder, B.J.: A hydrodynamically correct thermal lattice Boltzmann model. J. Stat. Phys. **97**, 1111–1121 (1997)
12. Massaioli, F., Benzi, R., Succi, S.: Exponential tails in two-dimensional Rayleigh-Bénard convection. Europhys. Lett. **21**, 305–310 (1993)
13. Mezrhab, A., Moussaoui, M.A., Jami, M., Naji, H., Bouzidi, M.: Double MRT thermal lattice Boltzmann method for simulating convective flows. Phys. Lett. A **374**, 3499–3507 (2010)

14. Kuznik, F., Rusaouen, G.: Numerical prediction of natural convection occurring in building components: a double-population lattice Boltzmann method. Numer. Heat Tr. A-Appl. **52**, 315–335 (2007)
15. Kuznik, F., Vareilles, J., Rusaouen, G., Krauss, G.: A double-population lattice Boltzmann method with non-uniform mesh for the simulation of natural convection in a square cavity. Int. J. Heat Fluid Flow **28**, 862–870 (2007)
16. Lallemand, P., Luo, L.-S.: Hybrid finite-difference thermal lattice Boltzmann equation. Int. J. Mod. Phys. B. **17**, 41–47 (2003)
17. Béghein, C., Haghighat, F., Allard, F.: Numerical study of double diffusive natural convection in a square cavity. Int. J. Heat Mass Transf. **35**, 833–846 (1992)
18. Morega, A., Nishimura, T.: Double diffusive convection by Chebyshev collocation method. Technol. Rep. Univ. **5**, 259–276 (1996)
19. Makayssi, T., Lamsaadi, M., Naimi, M., Hasnaoui, M., Raji, A., Bahlaoui, A.: Natural double diffusive convection in a shallow horizontal rectangular cavity uniformly heated and salted from the side and filled with non-Newtonian power-law fluids: the cooperating case. Energy Convers. Manag. **49**, 2016–2025 (2008)
20. Alleborn, N., Raszillier, H., Durst, F.: Lid-driven cavity with heat and mass transport. In. J. Heat Mass Transf. **42**, 833–853 (1999)
21. All-Amiri, A.M., Khanafer, K.M., Pop, I.: Numerical simulation of combined thermal and mass transport in a square lid-driven cavity. In. J. Ther. Sci. **46**, 622–671 (2007)
22. Teamah, M.A., El-Maghlany, W.M.: Numerical simulation of double-diffusive mixed convective flow in rectangular enclosure with insulated moving lid. Int. J. Ther. Sci. **49**, 1625–1638 (2010)
23. Mansour, A., Amahmid, A., Hasnaoui, M., Bourich, M.: Soret effect on double diffusive multiple solutions in a square porous cavity subject to cross gradients of temperature and concentration. Int. Comm. Heat Mass Transfer **31**, 431–440 (2004)
24. Bennacer, R., Mahidjiba, A., Vasseur, P., Beji, H., Duval, R.: The Soret effect on convection in a horizontal porous domain under cross-temperature and concentration gradients. Int. J. Numer. Methods Heat. Fluid. Flow **13**, 199–215 (2003)
25. Rebai, L.K., Mojtabi, A., Safi, M.J., Mohamad, A.A.: Numerical study of thermosolutal convection with soret effect in a square cavity. Int. J. Numer. Methods Heat. Fluid. Flow **18**, 561–574 (2008)
26. Bahloul, A., Boutana, N., Vasseur, P.: Double-diffusive and Soret-induced convection in a shallow horizontal porous layer. J. Fluid Mech. **491**, 325–352 (2003)
27. Khadiri, A., Amahmid, A., Hasnaoui, M., Rtibi, A.: Soret effect on double-diffusive convection in a square porous cavity heated and salted from below. Numer. Heat Transf. A **57**, 848–868 (2010)
28. Joly, F., Vasseur, P., Labrosse, G.: Soret-driven thermosolutal convection in a vertical enclosure. Int. Comm. Heat Mass Transfer **27**, 755–764 (2000)
29. Tsai, R., Huang, J.S.: Numerical study of Soret and dufour effects on heat and mass transfer from natural convection flow over a vertical porous medium with variable wall heat fluxes. Comput. Mater. Sci. **47**, 23–30 (2009)
30. Nader Ben Cheikh: Rrahim Ben Beya, Taieb Lili, Benchmark solution for time-dependent natural convection flows with an accelerated full-multigrid method. Num. Heat. transfer. prat B **52**, 131–151 (2007)